ADVANCES IN ATMOSPHERIC SCIENCES, VOL. 32, MAY 2015, 635–647

Investigation of the Mei-yu Front Using a New Deformation Frontogenesis Function

YANG Shuai*[1], GAO Shouting[1,2], and Chungu LU[3]

[1]*Laboratory of Cloud-Precipitation Physics and Severe Storms, Institute of Atmospheric Physics, Chinese Academy of Sciences, Beijing* 100029

[2]*State Key Laboratory of Severe Weather, Chinese Academy of Meteorological Sciences, Beijing* 100081

[3]*U.S. National Science Foundation, Arlington VA* 22230, *USA*

(Received 1 July 2014; revised 7 September 2014; accepted 15 September 2014)

ABSTRACT

A new frontogenesis function is developed and analyzed on the basis of a local change rate of the absolute horizontal gradient of the resultant deformation. Different from the traditional frontogenesis function, the newly defined deformation frontogenesis is derived from the viewpoint of dynamics rather than thermodynamics. Thus, it is more intuitive for the study of frontogenesis because the compaction of isolines of both temperature and moisture can be directly induced by the change of a flow field. This new frontogenesis function is particularly useful for studying the mei-yu front in China because mei-yu rainbands typically consist of a much stronger moisture gradient than temperature gradient, and involve large deformation flow. An analysis of real mei-yu frontal rainfall events indicates that the deformation frontogenesis function works remarkably well, producing a clearer mei-yu front than the traditional frontogenesis function based on a measure of the potential temperature gradient. More importantly, the deformation frontogenesis shows close correlation with the subsequent (6 h later) precipitation pattern and covers the rainband well, bearing significance for the prognosis or even prediction of future precipitation.

Key words: deformation, frontogenesis, precipitation

Citation: Yang, S., S. T. Gao, and C. G. Lu, 2014: Investigation of the mei-yu front using a new deformation frontogenesis function. *Adv. Atmos. Sci.*, **32**(5), 635–647, doi: 10.1007/s00376-014-4147-7.

1. Introduction

Frontogenesis has been studied widely for many years due to its importance in weather analyses and forecasting (Margules, 1906; Bergeron, 1928; Newton, 1954; Reed, 1955; Reed and Danielsen, 1958; Hoskins and Bretherton, 1972; Fang and Wu, 1998, 2001; Schultz and Steenburgh, 1999; Wu and Fang, 2001; Schultz and Sanders, 2002; Schultz and Trapp, 2003; Wu et al., 2004; Li et al., 2013). From a kinematic point of view, Petterssen (1936, 1956) defined the scalar frontogenesis function as the Lagrangian change of the magnitude of horizontal potential temperature gradient $d|\nabla\theta|/dt$. Miller (1948) discussed the change of front intensity by analyzing the scalar quantity. Keyser et al. (1988) extended Petterssen's frontogenesis function to vector form $d(\nabla\theta)/dt$, which is divided into the frontogenetical (or scalar) component $F_n = (1/2)|\nabla\theta|(D - E\cos 2\delta)$ and rotational component $F_s = (1/2)|\nabla\theta|(\zeta + E\sin 2\delta)$ with D, ζ and E denoting divergence, vorticity and resultant deformation, respectively, and δ representing the angle between the dilatation-axis orientation and the isentrope in the horizontal plane [$0^\circ < \delta < 90^\circ$; Keyser et al. (1988), Fig. 1]. Note that the F_n formula is given with the addition of the minus sign on Petterssen's scalar frontogenesis function.

Inspection of the definitions of scalar and vector frontogenesis functions reveals the significance of deformation in frontogenesis. Divergence and vorticity contribute to F_n and F_s respectively, while deformation works in both frontogenesis components. Furthermore, D and ζ may be positive or negative, and therefore the roles of D in F_n and ζ in F_s are determined by their signs. However, $E(=\sqrt{E_{\rm st}^2+E_{\rm sh}^2})$ is always positive regardless of the sign of stretching deformation $E_{\rm st}$ and shearing deformation $E_{\rm sh}$. Thus, the role of E is completely determined by the angle δ. As $\delta > 45^\circ$, deformation leads to F_s frontogenesis by rotating isentropes toward the dilatation axis, which makes δ tend to be less than 45°. Certainly, it is well known that deformation is frontogenetical in F_n provided that $\delta < 45^\circ$. In other words, in classical frontogenesis theory, deformation can either make the isolines of potential temperature tend to compact due to flow confluence, or it leads to frontogenesis by causing the angle between iso-

* Corresponding author: YANG Shuai
Email: ys_ys@126.com

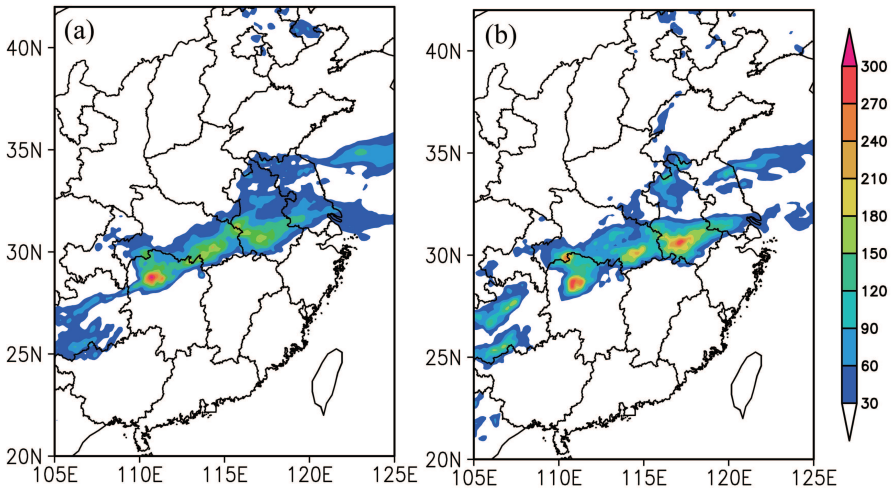

Fig. 1. (a) Observed and (b) simulated 48 h total rainfall amount (mm) over the middle and lower reaches of the Yangtze River from 0000 UTC 10 to 0000 UTC 12 July 2010.

lines of potential temperature and the dilation axis to rotate towards a favorable configuration for frontogenesis. Therefore, deformation is an important flow pattern for frontogenesis.

The importance of deformation in frontogenesis has been discussed in many studies. Sawyer (1956) and Eliassen (1962) derived the frontal secondary circulation equation by adopting a geostrophic approximation with the assumption of no change of potential temperature along a front. They illuminated the roles of terms associated with geostrophic deformation and shear deformation in frontal secondary circulation. Both Davies-Jones (1982, 1985) and Doswell (1984) studied the role of deformation in frontogenesis. Ninomiya (1984, 2000) showed that the deformation in the subtropical zone is also a primary contributor to mei-yu frontogenesis. Schultz et al. (1998) addressed the role of large-scale diffluent and confluent flow in low-level cyclone/front structure and evolution through a combined observational and idealized modeling approach. Gao et al. (2008) demonstrated the confluence effect of the resultant deformation (termed "total deformation" in their study) on moisture transport by both an idealized non-divergent and irrotational deformation flow pattern and case studies of heavy precipitation events associated with deformation-dominant flow.

The above-mentioned studies and theories emphasize the role of deformation in frontogenesis. However, previous studies have been based on the classical thermodynamic frontogenesis function, which relies on the Lagrangian change of potential temperature (θ) or equivalent potential temperature (θ_e) gradients (e.g., Ninomiya, 1984) as the criterion for frontogenesis/frontolysis (Petterssen, 1936, 1956; Davies-Jones, 1982; Doswell, 1984; Davies-Jones, 1985; Keyser et al., 1988). In such a defined frontogenesis function, a different tracer, θ or θ_e, must be adopted for either a temperature front or a moisture front. On the other hand, the confluence of airflow induced by deformation can drive the isolines of both temperature and moisture close together, dynamically, implying that deformation may have a key role in frontogenesis (Keyser et al., 1986, 1988). Furthermore, for certain types of precipitation systems, such as those associated with the mei-yu front in eastern China, the large-scale flow pattern often exhibits a dominant deformation pattern at low levels (Yang et al., 2007; Ran et al., 2009; Yang et al., 2009; Gao et al., 2010; Yang et al., 2014), while the divergence and vorticity are sometimes of smaller magnitude (Gao et al., 2008). In addition, a deformation and confluence shear line frequently presents in a mei-yu front and its associated frontal precipitation in eastern China. For these types of systems, it is important to understand the role of deformation, in the triggering and maintenance of the precipitation, and to gain insight into the temporal evolution of the deformation frontogenesis process and its correlation with precipitation.

In the present study, a deformation frontogenesis function is developed and applied to real meteorological cases. Different from the traditional frontogenesis equation, which evaluates a local change rate of the absolute horizontal gradient of potential (or equivalent potential) temperature, we derive a frontogenesis function by using a local change rate of the absolute horizontal gradient of resultant deformation. This new function is more intuitive and essential in dynamics compared to the traditional function, since it is the wind field that drives the compactness of isolines of temperature and moisture. In section 2, the dynamic connections and interactions among resultant deformation, the horizontal gradient of θ_e, and the vertical motion ω are elucidated. In sections 3 and 4, the expressions of deformation frontogenesis function are derived. The results from diagnoses and analyses of the deformation frontogenesis process in real mei-yu frontal episodes are reported in section 5. Conclusions are given in section 6.

2. Deformation-induced geostrophic circulation

Deformation is important in frontogenesis through shearing and stretching effects. It is conceivable that flow shearing

and stretching can cause an increase in the horizontal temperature gradient, and therefore baroclinicity through advection, which leads to frontogenesis. Such effects will act upon any physical variable, regardless of whether it is temperature or atmospheric moisture. However, the question is: Can such horizontal variability in flow fields result in circulations in the vertical direction (an essential dynamics feature typifying baroclinicity)? To elucidate the dynamic connections and interactions among deformation, the horizontal gradient of θ_e, and vertical motion ω, we conduct the following analysis using quasigeostrophic dynamics.

In the formulation of the quasigeostrophic ω equation, two "primary forcing functions" —differential vorticity advection and temperature advection—are considered (e.g., Bluestein, 1992). These forcing functions can be written as

$$-\frac{f_0}{\sigma}\frac{\partial}{\partial p}[-\boldsymbol{V}_g\cdot\nabla_p(\zeta_g+f)]-\frac{R}{\sigma p}\nabla_p^2(-\boldsymbol{V}_g\cdot\nabla_p T)\,, \quad (1)$$

where $\boldsymbol{V}_g$ and ζ_g are quasigeostrophic velocity vector and vertical relative vorticity, f and f_0 are Coriolis parameter and its constant approximation, σ is static stability parameter, T is absolute temperature, R is ideal gas constant, and other notations are standard meteorological notation, and the problem is analyzed in a p vertical coordinate.

The differential vorticity-advection term, i.e., the first term in Eq. (1), can be separated into the following two parts:

$$-\frac{f_0}{\sigma}\left[-\frac{\partial\boldsymbol{V}_g}{\partial p}\cdot\nabla_p(\zeta_g+f)-\boldsymbol{V}_g\cdot\nabla_p\frac{\partial\zeta_g}{\partial p}\right]\,. \quad (2)$$

The first term in Eq. (2) represents advection of geostrophic absolute vorticity by thermal wind. The second term represents advection of thermal vorticity by geostrophic wind. The temperature-advection term [the second term in Eq. (1)] can be expanded similarly:

$$-\frac{R}{\sigma p}[-\nabla_p^2\boldsymbol{V}_g\cdot(\nabla_p T)-\boldsymbol{V}_g\cdot\nabla_p(\nabla_p^2 T)]\,. \quad (3)$$

Using the thermal-wind relation

$$\begin{cases} -\dfrac{\partial v_g}{\partial p}=\dfrac{R}{f}\dfrac{1}{p}\left(\dfrac{\partial T}{\partial x}\right)_p & (4a)\\ -\dfrac{\partial u_g}{\partial p}=-\dfrac{R}{f}\dfrac{1}{p}\left(\dfrac{\partial T}{\partial y}\right)_p\,, & (4b)\end{cases}$$

and enduring some algebraic manipulations, we find that the temperature-advection term [Eq. (3)] can be broken up into the following three parts:

$$\frac{f_0}{\sigma}\left[\frac{\partial\boldsymbol{V}_g}{\partial p}\cdot\nabla_p\zeta_g+\left(-\boldsymbol{V}_g\cdot\nabla_p\frac{\partial\zeta_g}{\partial p}\right)+\left(E_{\mathrm{sh},g}\frac{\partial E_{\mathrm{st},g}}{\partial p}-E_{\mathrm{st},g}\frac{\partial E_{\mathrm{sh},g}}{\partial p}\right)\right]\,, \quad (5)$$

where the relation $\partial u_g/\partial x+\partial v_g/\partial y=0$ has been used, and the geostrophic stretching and shearing deformation are respectively in the form

$$E_{\mathrm{st},g}=\frac{\partial u_g}{\partial x}-\frac{\partial v_g}{\partial y}\,,\quad E_{\mathrm{sh},g}=\frac{\partial v_g}{\partial x}+\frac{\partial u_g}{\partial y}\,.$$

One can see that the first two terms in Eq. (5) are now being converted to similar terms in Eq. (2), which means that the parts of thermal advection are physically equivalent to the corresponding parts of vorticity advection. The equability of temperature and vorticity advection is a well-known concept in synoptic meteorology. However, the most important result from the above derivation comes from the third term in Eq. (5), which presents an additional forcing mechanism for vertical motion. This forcing measures the net effect of the permutation of shearing/stretching and thermal shearing/stretching deformation.

Combining the vorticity-advection and temperature-advection forcing functions using Eqs. (2) and (5), one can obtain the following frictionless and adiabatic form of the quasigeostrophic ω-equation:

$$\left(\nabla_p^2+\frac{f_0^2}{\sigma}\frac{\partial^2}{\partial p^2}\right)\omega=\frac{f_0}{\sigma}\left[2\left(\frac{\partial\boldsymbol{V}_g}{\partial p}\cdot\nabla_p\zeta_g\right)+\frac{\partial\boldsymbol{V}_g}{\partial p}\cdot\nabla_p f-\left(E_{\mathrm{sh},g}\frac{\partial E_{\mathrm{st},g}}{\partial p}-E_{\mathrm{st},g}\frac{\partial E_{\mathrm{sh},g}}{\partial p}\right)\right]\,. \quad (6)$$

This equation implies a circulation in the vertical plane within the geostrophic dynamics framework. The vertical differential advection of vorticity, and the vertical differential stretching and shearing deformation in the horizontal wind can all contribute a vertical motion.

Because a frontal circulation can be directly related to a configuration of the deformation field, it is dynamically more sensible to adopt deformation as a key variable to examine frontogenesis/frontollysis. As mentioned in the previous section, it does not matter what dynamical tracer, be it θ or θ_e, is involved in a particular frontal circulation, as long as a flow feature that transports these tracers is captured. The deformation-induced difference in vertical motion inside and outside the frontal zone makes a difference in the pumping up of low-level air, which will cause low-level convergence and thus increase the horizontal gradient of θ_e. Therefore, the connections and interactions among E, θ_e and ω develop.

3. Derivation of the deformation frontogenesis function

From the above analyses, one can see that flow deformation may serve as a precursor for dynamic frontogenesis and a driving factor for any dynamical tracer to be concentrated upon. Therefore, it is reasonable to define a frontogenesis function using a deformation field. Such a defined frontogenesis function will be independent of the tracer type, and thus can be used in situations where a temperature/moisture front occurs in the absence of a moisture/temperature front. However, since a frontal circulation may be forced by both shear-

ing and stretching deformation, we need to define a more general field to include the effects of both.

Based on Petterssen's velocity decomposition (1956), the 2D velocity-differential tensor can be written as

$$\frac{\partial u_i}{\partial x_j} = \nabla \boldsymbol{V} = \frac{1}{2}\begin{pmatrix} E_{\rm st} & E_{\rm sh} \\ E_{\rm sh} & -E_{\rm st} \end{pmatrix} + \frac{1}{2}\begin{pmatrix} D & 0 \\ 0 & D \end{pmatrix} + \frac{1}{2}\begin{pmatrix} 0 & \zeta \\ -\zeta & 0 \end{pmatrix}, \tag{7}$$

where $u_i=(u,v)$ and $\partial x_j=(\partial x,\partial y)$. The velocity-differentials $D=(\partial u/\partial x+\partial v/\partial y)$, $\zeta=(\partial v/\partial x-\partial u/\partial y)$, $E_{\rm st}=(\partial u/\partial x-\partial v/\partial y)$, and $E_{\rm sh}=(\partial v/\partial x+\partial u/\partial y)$ are, respectively, the divergence, vorticity, stretching deformation, and shearing deformation.

For the first matrix on the right-hand side of Eq. (7), a resultant deformation is defined to generalize the resultant effect of both stretching and shearing deformations. In order to do so, we take determinant for the first matrix and the resultant deformation can thus be defined as

$$E = \sqrt{E_{\rm st}^2 + E_{\rm sh}^2}\,. \tag{8}$$

The resultant deformation has been used by meteorologists for many decades (e.g., Petterssen, 1956; Keyser et al., 1986; Norbury, 2002). When the (x,y) coordinate system is rotated to a new coordinate system (x',y'), it can be proven that the resultant deformation preserves symmetry under a coordinate rotation. That is, the resultant deformation is independent of the coordinate rotation.

With the resultant deformation defined above, we can now introduce a deformation frontogenesis function, using the traditional method of measuring frontogenesis, i.e.,

$$F = \frac{\partial}{\partial t}|\nabla E|\,, \tag{9}$$

where E is the resultant deformation, and $|\nabla E|$ represents the absolute value of the horizontal gradient of resultant deformation, which can be written $|\nabla E| = \sqrt{(\partial E/\partial x)^2+(\partial E/\partial y)^2}$.

Note that the operator $\partial/\partial t$ (but not d/dt) is utilized in Eq. (9) in the present study, which is based on two points. First, Wu et al. (2004) discussed the intensity change of frontal systems by utilizing both local and Lagrangian frontogenesis functions, and then further studied the problem of geostrophic adjustment during frontogenesis. Obviously, local frontogenesis has already been used in the past. Second, the resultant deformation E acted by operator $\partial/\partial t$ herein is just a driver (from the dynamical viewpoint) but not a tracer (in the thermodynamic sense).

Beginning from horizontal motion equations, Gao et al. (2008) derived a prognostic equation of the resultant deformation:

$$\begin{aligned} \frac{\partial E}{\partial t} = {} & \underbrace{-\boldsymbol{V}_h\cdot\nabla E}_{A_1} \underbrace{-\omega\frac{\partial E}{\partial p}}_{A_2} \underbrace{-ED}_{A_3} + \underbrace{E^{-1}\beta(uE_{\rm st}+vE_{\rm sh})}_{A_4} - \\ & \underbrace{E^{-1}E_{\rm st}\left(\frac{\partial^2\phi}{\partial x^2}-\frac{\partial^2\phi}{\partial y^2}\right)}_{A_5} - \underbrace{E^{-1}E_{\rm sh}\left(2\frac{\partial^2\phi}{\partial x\partial y}\right)}_{A_6} - \\ & \underbrace{E^{-1}E_{\rm st}\left(\frac{\partial\omega}{\partial x}\frac{\partial u}{\partial p}-\frac{\partial\omega}{\partial y}\frac{\partial v}{\partial p}\right)}_{A_7} - \\ & \underbrace{E^{-1}E_{\rm sh}\left(\frac{\partial\omega}{\partial y}\frac{\partial u}{\partial p}+\frac{\partial\omega}{\partial x}\frac{\partial v}{\partial p}\right)}_{A_8} + \\ & \underbrace{E^{-1}E_{\rm st}\left(\frac{\partial F_x}{\partial x}-\frac{\partial F_y}{\partial y}\right)}_{A_9} + \underbrace{E^{-1}E_{\rm sh}\left(\frac{\partial F_x}{\partial y}+\frac{\partial F_y}{\partial x}\right)}_{A_{10}} \underbrace{}_{A_{11}}. \end{aligned} \tag{10}$$

It can be seen from Eq. (10) that the local time rate of change of resultant deformation is related to the advection of deformation (both horizontally and vertically: A_2 and A_3), is produced by the interaction of deformation and divergence (A_4), is affected by the β effect (A_5), and is related to various second-order derivatives of geopotential acting on the stretching and shearing deformations (A_6 and A_7), the tilting effects (A_8 and A_9), and friction and/or turbulence mixture (A_{10} and A_{11}). Furthermore, by the effects of A_8 and A_9, the influence of vertical motion on E is present.

On the basis of the above resultant deformation equation, the deformation frontogenesis function is derived in detail:

Rewrite $|\nabla E|$ to $\sqrt{(\nabla E)^2}$ and, using the derivative chain rule, Eq. (6) can be decomposed into

$$F = \frac{\partial}{\partial t}|\nabla E| = \frac{1}{|\nabla E|}\left[\frac{\partial E}{\partial x}\frac{\partial}{\partial t}\left(\frac{\partial E}{\partial x}\right)+\frac{\partial E}{\partial y}\frac{\partial}{\partial t}\left(\frac{\partial E}{\partial y}\right)\right], \tag{11}$$

where $|\nabla E|\neq 0$ is assumed.

Let us write Eq. (10) in symbolic form,

$$\frac{\partial E}{\partial t} = A_2+A_3+A_4+A_5+A_6+A_7+A_8+A_9+A_{10}+A_{11}\,, \tag{12}$$

where $A_2, A_3, \cdots, A_{11}$ are the terms in Eq. (10). Thus, Eq. (11) becomes

$$\begin{aligned} F &= \frac{1}{|\nabla E|}\left\{\frac{\partial E}{\partial x}\left[\frac{\partial}{\partial x}\left(\frac{\partial E}{\partial t}\right)\right]+\frac{\partial E}{\partial y}\left[\frac{\partial}{\partial y}\left(\frac{\partial E}{\partial t}\right)\right]\right\} \\ &= \frac{1}{|\nabla E|}[\nabla E\cdot\nabla(A_2+A_3+A_4+A_5+A_6+A_7+A_8+A_9+A_{10}+A_{11})] \\ &= -\boldsymbol{V}\cdot\nabla_3|\nabla E| - \frac{1}{|\nabla E|}\left[\frac{\partial E}{\partial x}\left(\frac{\partial \boldsymbol{V}_h}{\partial x}\cdot\nabla E\right)+\frac{\partial E}{\partial y}\left(\frac{\partial \boldsymbol{V}_h}{\partial y}\cdot\nabla E\right)\right] - \\ &\quad \frac{1}{|\nabla E|}\left(\frac{\partial E}{\partial x}\frac{\partial\omega}{\partial x}+\frac{\partial E}{\partial y}\frac{\partial\omega}{\partial y}\right)\frac{\partial E}{\partial p}+\frac{1}{|\nabla E|}\left(\frac{\partial E}{\partial x}\frac{\partial}{\partial x}+\frac{\partial E}{\partial y}\frac{\partial}{\partial y}\right)(A_4+A_5+A_6+A_7+A_8+A_9+A_{10}+A_{11}) \end{aligned}$$

$$= -\boldsymbol{V}\cdot\nabla_3|\nabla E| - \frac{1}{|\nabla E|}\left[\frac{1}{2}E_{\rm st}\left(\frac{\partial E}{\partial x}\right)^2 + E_{\rm sh}\left(\frac{\partial E}{\partial x}\frac{\partial E}{\partial y}\right) - \frac{1}{2}E_{\rm st}\left(\frac{\partial E}{\partial y}\right)^2\right] -$$
$$\frac{1}{2}D|\nabla E| - \frac{1}{|\nabla E|}\left(\frac{\partial E}{\partial x}\frac{\partial \omega}{\partial x} + \frac{\partial E}{\partial y}\frac{\partial \omega}{\partial y}\right)\frac{\partial E}{\partial p} + \frac{1}{|\nabla E|}\left(\frac{\partial E}{\partial x}\frac{\partial}{\partial x} + \frac{\partial E}{\partial y}\frac{\partial}{\partial y}\right)(A_4 + A_5 + A_6 + A_7 + A_8 + A_9 + A_{10} + A_{11})$$
$$= F_1 + F_2 + F_3 + F_4 + F_5 + F_6 + F_7, \tag{13}$$

where

$$F_1 = -\boldsymbol{V}\cdot\nabla_3|\nabla E|$$
$$F_2 = -\frac{1}{|\nabla E|}\left[\frac{1}{2}E_{\rm st}\left(\frac{\partial E}{\partial x}\right)^2 + E_{\rm sh}\left(\frac{\partial E}{\partial x}\frac{\partial E}{\partial y}\right) - \frac{1}{2}E_{\rm st}\left(\frac{\partial E}{\partial y}\right)^2\right]$$
$$F_3 = \frac{1}{|\nabla E|}\left(\frac{\partial E}{\partial x}\frac{\partial}{\partial x} + \frac{\partial E}{\partial y}\frac{\partial}{\partial y}\right)A_4 - \frac{1}{2}D|\nabla E|$$
$$= -\frac{3}{2}D|\nabla E| - \frac{E}{|\nabla E|}(\nabla E\cdot\nabla D)$$
$$F_4 = \frac{1}{|\nabla E|}\left(\frac{\partial E}{\partial x}\frac{\partial}{\partial x} + \frac{\partial E}{\partial y}\frac{\partial}{\partial y}\right)A_5 = \frac{1}{|\nabla E|}(\nabla E\cdot\nabla A_5)$$
$$F_5 = \frac{1}{|\nabla E|}\left(\frac{\partial E}{\partial x}\frac{\partial}{\partial x} + \frac{\partial E}{\partial y}\frac{\partial}{\partial y}\right)(A_6 + A_7)$$
$$= \frac{1}{|\nabla E|}[\nabla E\cdot\nabla(A_6 + A_7)]$$
$$F_6 = \frac{1}{|\nabla E|}\left(\frac{\partial E}{\partial x}\frac{\partial}{\partial x} + \frac{\partial E}{\partial y}\frac{\partial}{\partial y}\right)(A_8 + A_9) -$$
$$\frac{1}{|\nabla E|}\left(\frac{\partial E}{\partial x}\frac{\partial \omega}{\partial x} + \frac{\partial E}{\partial y}\frac{\partial \omega}{\partial y}\right)\frac{\partial E}{\partial p}$$
$$= \frac{1}{|\nabla E|}\left[\nabla E\cdot\nabla(A_8 + A_9) - (\nabla E\cdot\nabla\omega)\frac{\partial E}{\partial p}\right]$$
$$F_7 = \frac{1}{|\nabla E|}\left(\frac{\partial E}{\partial x}\frac{\partial}{\partial x} + \frac{\partial E}{\partial y}\frac{\partial}{\partial y}\right)(A_{10} + A_{11})$$
$$= \frac{1}{|\nabla E|}[\nabla E\cdot\nabla(A_{10} + A_{11})]. \tag{14}$$

In Eqs. (12–14), $\boldsymbol{V}$ is a three-dimensional velocity vector, $\nabla_{\rm h}\cdot\boldsymbol{V}$ is horizontal divergence, and $\omega = dp/dt$ is the vertical velocity in the p-coordinate system.

According to Eq. (13), F_1 represents the contribution of the advection of the absolute value of the horizontal total deformation gradient to local frontogenesis. The sign of this term is determined by projection of the 3D velocity vector on the gradient of $|\nabla E|$. As the angle between $\boldsymbol{V}$ and $\nabla_3|\nabla E|$ is less than $\pi/2$, the projection is positive, $F_1 < 0$, and advection leads to frontolysis. Otherwise, $F_1 > 0$ leads to frontogenesis. In addition, the deformation frontogenesis equation is also associated with horizontal deformation (F_2), horizontal divergence (F_3), the β effect (F_4), pressure gradient force (F_5), the tilting effect (F_6), and friction and/or turbulence mixture (F_7).

4. Alternative derivation of the deformation frontogenesis function

In section 3, the deformation frontogenesis function [Eq. (13)] was derived based on the resultant deformation equation [Eq. (10)] of Gao et al. (2008). However, both equations include too many terms, which increase their complexity. At least in form, the advantage of the above deformation frontogenesis function [Eq. (13)] is not too evident compared with the traditional frontogenesis function. Therefore, simplification, or another derivation, is necessary to cut down the complexity of the deformation frontogenesis function. An alternative derivation of the deformation frontogenesis function is performed as follows:

The horizontal motion equation and its component forms can be written as

$$\frac{\partial \boldsymbol{V}_{\rm h}}{\partial t} = \underbrace{-(\boldsymbol{V}\cdot\nabla_3)\boldsymbol{V}_{\rm h}}_{\boldsymbol{J}_1} \underbrace{-\nabla\phi}_{\boldsymbol{J}_2} \underbrace{-2\Omega\times\boldsymbol{V}}_{\boldsymbol{J}_3} + \underbrace{\boldsymbol{F}}_{\boldsymbol{J}_4}, \tag{15a}$$
$$\frac{\partial u}{\partial t} = \underbrace{-(\boldsymbol{V}\cdot\nabla_3)u}_{J_{x,1}} \underbrace{-\frac{\partial\phi}{\partial x}}_{J_{x,2}} \underbrace{+fv}_{J_{x,3}} \underbrace{+F_x}_{J_{x,4}}, \tag{15b}$$
$$\frac{\partial v}{\partial t} = \underbrace{-(\boldsymbol{V}\cdot\nabla_3)v}_{J_{y,1}} \underbrace{-\frac{\partial\phi}{\partial y}}_{J_{y,2}} \underbrace{-fu}_{J_{y,3}} \underbrace{+F_y}_{J_{y,4}}, \tag{15c}$$

with $\boldsymbol{J} = \sum_{m=1}^{4}\boldsymbol{J}_m$, $J_x = \sum_{m=1}^{4}J_{x,m}$, $J_y = \sum_{m=1}^{4}J_{y,m}$, $\boldsymbol{V}_h = u\boldsymbol{i} + v\boldsymbol{j}$ and $\boldsymbol{J} = J_x\boldsymbol{i} + J_y\boldsymbol{j}$; $J_{x,m}$ and $J_{y,m}(m = 1,2,3,4)$ are the forcing terms of the local change of horizontal wind components.

From Eq. (8), we have

$$\frac{\partial E}{\partial t} = \frac{1}{E}\left(E_{\rm st}\frac{\partial E_{\rm st}}{\partial t} + E_{\rm sh}\frac{\partial E_{\rm sh}}{\partial t}\right). \tag{16}$$

Combining with Eq. (15), $\partial E_{\rm st}/\partial t$ and $\partial E_{\rm sh}/\partial t$ in Eq. (16) become

$$\frac{\partial E_{\rm st}}{\partial t} = \frac{\partial}{\partial t}\left(\frac{\partial u}{\partial x} - \frac{\partial v}{\partial y}\right) = \frac{\partial}{\partial x}\left(\frac{\partial u}{\partial t}\right) - \frac{\partial}{\partial y}\left(\frac{\partial v}{\partial t}\right)$$
$$= \frac{\partial J_x}{\partial x} - \frac{\partial J_y}{\partial y} = J_{\rm st},$$
$$\frac{\partial E_{\rm sh}}{\partial t} = \frac{\partial}{\partial t}\left(\frac{\partial v}{\partial x} + \frac{\partial u}{\partial y}\right) = \frac{\partial}{\partial x}\left(\frac{\partial v}{\partial t}\right) + \frac{\partial}{\partial y}\left(\frac{\partial u}{\partial t}\right)$$
$$= \frac{\partial J_y}{\partial x} + \frac{\partial J_x}{\partial y} = J_{\rm sh}.$$

Note that, similarly, we have the relations

$$J_{{\rm st},m} = \frac{\partial J_{x,m}}{\partial x} - \frac{\partial J_{y,m}}{\partial y} \text{ and}$$
$$J_{{\rm sh},m} = \frac{\partial J_{y,m}}{\partial x} + \frac{\partial J_{x,m}}{\partial y} \text{ with } m = 1,2,3,4.$$

Thus, Eq. (16) becomes

$$\frac{\partial E}{\partial t} = \frac{1}{E}(E_{\rm st}J_{\rm st} + E_{\rm sh}J_{\rm sh}). \tag{17}$$

From Eq. (17), Eq. (11) can be rewritten as

$$F = \frac{\partial}{\partial t}|\nabla E| = \frac{1}{|\nabla E|}\left(\frac{\partial E}{\partial x}\frac{\partial}{\partial x} + \frac{\partial E}{\partial y}\frac{\partial}{\partial y}\right)\left(\frac{\partial E}{\partial t}\right)$$
$$= \frac{1}{|\nabla E|}(\nabla E \cdot \nabla)\left(\frac{\partial E}{\partial t}\right)$$
$$= \frac{1}{|\nabla E|}(\nabla E \cdot \nabla)\left[\frac{1}{E}(E_{\rm st}J_{\rm st} + E_{\rm sh}J_{\rm sh})\right] . \quad (18)$$

Equation (18) can be further simplified to

$$F = \boldsymbol{n} \cdot \nabla(\mathrm{tg}\alpha J_{\rm st} + \mathrm{ctg}\alpha J_{\rm sh}) , \quad (19)$$

with $\boldsymbol{n} = \nabla E/|\nabla E|$, $\mathrm{tg}\alpha = E_{\rm st}/E$ and $\mathrm{ctg}\alpha = E_{\rm sh}/E$.

For convenience of calculation and analysis, Eq. (19) is expanded and noted as the sum operator of several forcing factors $X_m (m = 1,2,3,4)$:

$$F = \sum_{m=1}^{4} X_m , \quad (20a)$$

where

$$X_m = \boldsymbol{n} \cdot \nabla(\mathrm{tg}\alpha J_{{\rm st},m} + \mathrm{ctg}\alpha J_{{\rm sh},m}), \quad m = 1,2,3,4 . \quad (20b)$$

In Eq. (20b), X_m denotes the co-action of two kinds of deformation effects. One is the deformation of the wind field itself ($\mathrm{tg}\alpha = E_{\rm st}/E$, $\mathrm{ctg}\alpha = E_{\rm sh}/E$), and the other is the stretching deformation ($J_{{\rm st},m}$) and shearing deformation ($J_{{\rm sh},m}$) of four forcing terms in the horizontal wind local change tendency equation [Eq. (15)]. Taking $m = 1$ (or $2,3,4$) as an example, the second type of deformation effect ($J_{{\rm st},m}$ and $J_{{\rm sh},m}$) represents the advection (or pressure gradient force, Coriolis force, friction and/or turbulence mixture) forcing deformation. For brevity, $X_m (m = 1,2,3,4)$ is termed advection forcing (X_1), pressure gradient forcing (X_2), Coriolis forcing (X_3), and friction forcing (X_4) of the deformation frontogenesis function.

This form of the deformation frontogenesis function [Eq. (20)], recorded as a sum operator, looks simple and offers an easy explanation relative to the expression [Eq. (13)] derived in section 3. Equation (20) includes four terms with a clear physical sense for each term. At least in form, it is not more complicated than the traditional frontogenesis function. Furthermore, it is not harder for it to provide a clear physical explanation for each forcing term in Eq. (20). Also, based on its advantage from the dynamic viewpoint (e.g., the confluence of airflow induced by deformation can dynamically drive the isolines of any one tracer, be it θ or θ_e, closer together), the deformation frontogenesis function will exert its maximal advantage if its diagnostic analysis for frontogenesis and associated precipitation via a case study is good.

The difference and relationship between Eqs. (13) and (20) should be discussed to develop contextual linkages, since the latter is an alternative form of the former. By rigorous derivation, we have the relations $X_1 = F_1 + F_2 + F_3 + F_6$, $X_2 = F_5$, $X_3 = F_4$, and $X_4 = F_7$. After careful derivation and repeated validation, it is shown that the above relations are rigorous and without any conditions of assumptions and simplifications. All these analyses indicate that, in addition to being concise in form, Eq. (20) can reflect all of the information contained in Eq. (13). Therefore, the calculation in the case study in the next section based on Eq. (20) can be considered reasonable.

Note that Eq. (13) is retained in the paper for two reasons:

(1) Because the deformation frontogenesis function F is defined as the local change rate of $|\nabla E|$, it is natural to derive F based on the E equation. It is logical to derive the E equation first, and then F based on the E equation. Furthermore, from E equation to its extended application (F), a set of complete and systematic derivation about deformation theory is built up, just as have done in the first author's Ph.D dissertation (Yang, 2007). Because too many terms are included in Eq. (13), Eq. (20) is derived as an alternative form of the deformation frontogenesis function.

(2) The origin of Eq. (13) is important as a "true" value to validate Eq. (20), both in theory and in calculation. By testing, Eq. (20) can reflect all of the information contained in Eq. (13). Therefore, their calculation results in a real case analysis are also consistent.

Certainly, Eq. (20) can be further simplified under certain conditions. For example, if pure stretching deformation is assumed (which can be achieved by rotating the coordinate system), $E_{\rm sh} = 0$ and $E = E_{\rm st}$, which lead to $\mathrm{tg}\alpha = 1$ and $\mathrm{ctg}\alpha = 0$. Therefore, Eq. (20b) becomes

$$X_m = \boldsymbol{n} \cdot \nabla J_{{\rm st},m} , \quad (21)$$

which leads to the frontogenesis function, Eqs. (20a) and (19), to become

$$F = \sum_{m=1}^{4} \boldsymbol{n} \cdot \nabla J_{{\rm st},m} = n \cdot \nabla J_{\rm st} . \quad (22)$$

At this moment, the shear deformations of both the wind field itself and the forcing terms of wind change disappear. Only the effects of their stretching deformations work. In the next section, a case study is reported in which we validate the application of the deformation frontogenesis function.

5. Case study

A heavy rainfall event associated with a mei-yu front occurred over the middle and lower reaches of the Yangtze River in China from 0000 UTC 10 to 0000 UTC 12 July 2010 (Fig. 1a). The rainband was oriented in the west-southwest to east-northeast direction. The circulation background was as follows. A line of strong confluence shear and a typical "saddle" flow pattern existed in the lower troposphere (Figs. 2a–c). This confluence shear zone was a result of the large-scale flow pattern that consisted of a subtropical high located in the northwestern Pacific, a low centered at (33.7°N, 118°E) and a southwest vortex at (28.7°N, 106.5°E), as well as another high at (34.5°N, 109°E) (Fig. 2a). The "saddle" flow pattern stretched vertically to the 600 hPa level (not shown).

Along this shear region, there was a zone of high equivalent potential temperature θ_e that clearly marked the mei-yu frontal zone stretching in the northeast–southwest direction

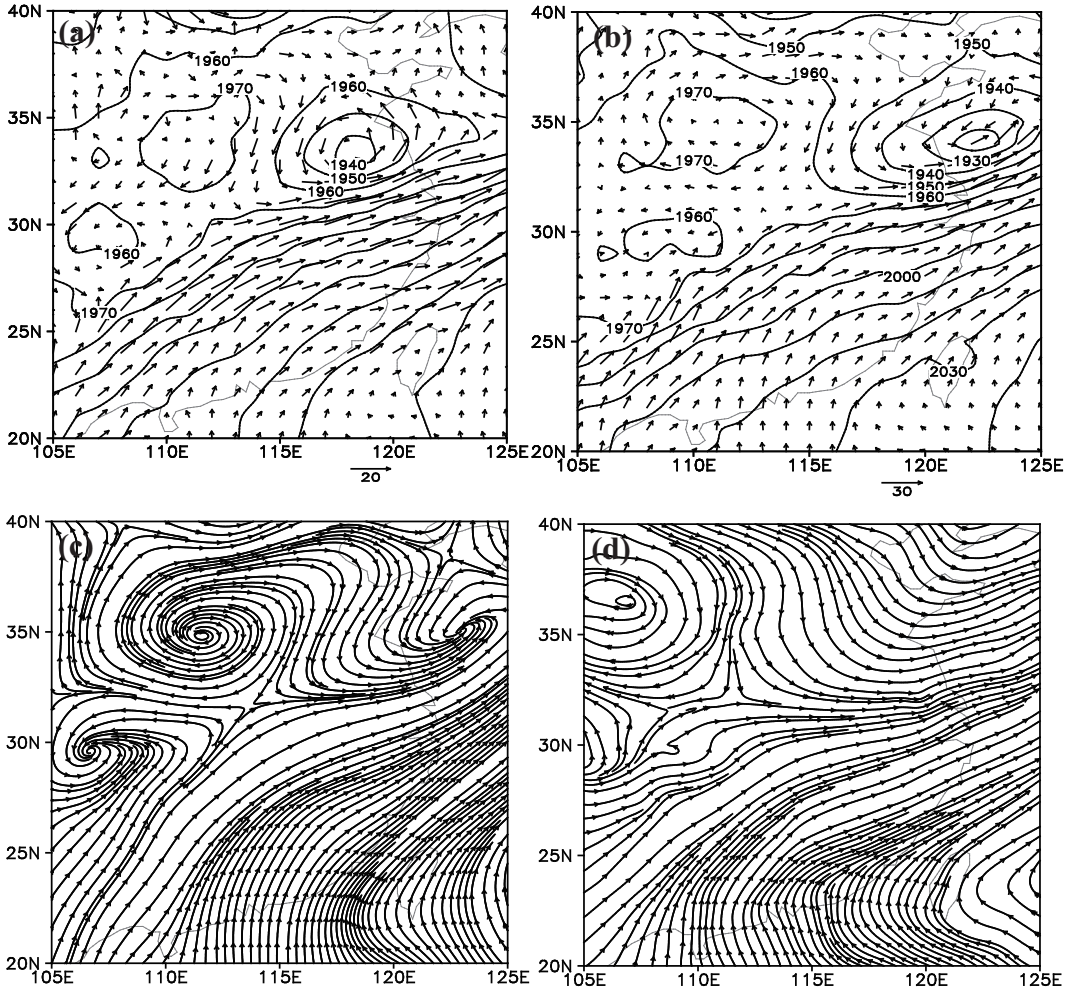

Fig. 2. Observed geopotential height fields (isolines, gpm) and wind vectors (m s^{-1}) at the 800 hPa level (a) at 0000 UTC 10 and (b) at 0000 UTC 11 July 2010. (c) Observed and (d) simulated streamline fields at the 800 hPa level at 1200 UTC 11 July 2010.

between 25°N and 36°N (Fig. 3a). In particular, Ninomiya (1984) argued that, different from polar frontogenesis where a gradient of potential temperature is conventionally used, a measure of frontogenesis in mei-yu rainbands should adopt a gradient of equivalent potential temperature. Therefore, the strong gradient of equivalent potential temperature is still used to denote the frontal zone, but the traditional frontogenesis function is replaced by the deformation frontogenesis function.

The fronts (with compact isolines of θ_e) formed before the onset of precipitation and maintained during the course of precipitation. Unlike the classical cold/warm front, this case showed a strong gradient in humidity but not in temperature over the middle and lower reaches of the Yangtze River in China (Figs. 3b and c).

To obtain a set of fine-scale data to perform the diagnosis of the frontogenesis function, the Weather Research and Forecasting (WRF) model is used to produce a mesoscale numerical simulation. Yu et al. (2012) simulated the rainfall event using the WRF model and obtained good results according to its validation. Therefore, the same configuration, schemes, initial and boundary fields are adopted in our simulation. The details of the configuration of the simulation can be found in Yu et al. (2012). The resolutions of the outer and inner domains of the simulation are 36 km and 12 km. The inner-domain model outputs are used to analyze the frontogenesis features for the case. Figure 1b shows the simulated 48-h precipitation between 0000 UTC 10 and 0000 UTC 12 July 2010. The orientations of rainbands between the simulation and observation are similar (Figs. 1a and b). The observed precipitation has a maximal center of 270 mm $(48\ h)^{-1}$, while the simulated precipitation has four centers of considerable strength [> 300 mm $(48\ h)^{-1}$]. The typical deformation stream field is also reproduced (Figs. 2c and d). The simulated geopotential height and temperature fields were validated in Fig. 2 of Yu et al. (2012). The model dataset is used to diagnose the frontogenesis function.

From the distribution of humidity (Fig. 3c), equivalent potential temperature (Fig. 3a), and the resultant deformation (Fig. 4a), we can see that the intense humidity gradient is closely correlated with a large value of the resultant deformation. The pattern, orientation and coverage of the large-value

regions between the resultant deformation and humidity consistently correspond with each other (Figs. 4a and 3c). Furthermore, the strength of the resultant deformation is nearly two times larger than vorticity/divergence in this case, reaching up to 1.0×10^{-4} s^{-1} (Fig. 4). On the basis of the above analyses, deformation was large in magnitude compared to vorticity and divergence, and showed a strong presence in the large humidity gradient regions. Thus, this was likely the driving factor for frontogenesis in the frontal rainfall case. With this analysis, the deformation frontogenesis process by taking accounting of the gradient of total deformation is justified and is examined below.

As a comparison, a traditional frontogenesis function using equivalent potential temperature was also calculated and analyzed. Following Ninomiya (1984, 2000) and Sun and Du (1996), this frontogenesis function can be written as

$$\mathrm{FG} = \frac{d|\nabla\theta_e|}{dt} = \mathrm{FG}_1 + \mathrm{FG}_2 + \mathrm{FG}_3 + \mathrm{FG}_4 \,, \qquad (23)$$

where $\mathrm{FG}_1, \mathrm{FG}_2, \mathrm{FG}_3$, and FG_4 are defined, respectively, as

$$\mathrm{FG}_1 = \frac{1}{|\nabla\theta_e|}\left[(\nabla\theta_e\cdot\nabla)\frac{d\theta_e}{dt}\right] \,,$$

$$\mathrm{FG}_2 = -\frac{1}{2}\frac{1}{|\nabla\theta_e|}(\nabla\theta_e)^2\left(\frac{\partial u}{\partial x}+\frac{\partial v}{\partial y}\right) \,,$$

$$\mathrm{FG}_3 = -\frac{1}{2}\frac{1}{|\nabla\theta_e|}\left[\left(\frac{\partial\theta_e}{\partial x}\right)^2-\left(\frac{\partial\theta_e}{\partial y}\right)^2\right]\left(\frac{\partial u}{\partial x}-\frac{\partial v}{\partial y}\right)+ 2\frac{\partial\theta_e}{\partial x}\frac{\partial\theta_e}{\partial y}\left(\frac{\partial v}{\partial x}+\frac{\partial u}{\partial y}\right) \,,$$

$$\mathrm{FG}_4 = -\frac{1}{|\nabla\theta_e|}\frac{\partial\theta_e}{\partial p}\left(\frac{\partial\theta_e}{\partial x}\frac{\partial\omega}{\partial x}+\frac{\partial\theta_e}{\partial y}\frac{\partial\omega}{\partial y}\right) \,,$$

where θ_e is equivalent potential temperature; and u, v, and ω are the zonal, meridional and vertical velocity components, respectively. $\mathrm{FG}_1, \mathrm{FG}_2, \mathrm{FG}_3$, and FG_4 are diabatic heating, convergence, deformation, and the slantwise terms, respectively.

From Fig. 5, the deformation frontogenesis zones [with the friction forcing term X_4 in Eq. (20) neglected] correspond fronts (compact equivalent potential temperature zone) better than the traditional frontogenesis zones [the calculation of the traditional frontogenesis function neglects the diabatic heating, i.e., FG_1 in Eq. (23)]. The pattern, orientation and coverage of the large-value regions between the deformation frontogenesis and θ_e gradients are consistent with each other (Figs. 5a, c and e), while the scattered distributions of traditional frontogenesis do not completely cover the compact regions of θ_e isolines (Figs. 5b, d and f). More importantly, the pattern of deformation frontogenesis and the rainband closely resemble each other (Figs. 5a, c and e, and Figs. 6a–c). For instance, the deformation frontogenesis regions and the interlinked double rainbands stretch northeastwards to the west of 115°E in Figs. 5a and 6a, while the traditional frontogenesis function cannot reflect the pattern of precipitation (Figs. 5b and d). The "Y-shaped" patterns of precipitation (red line

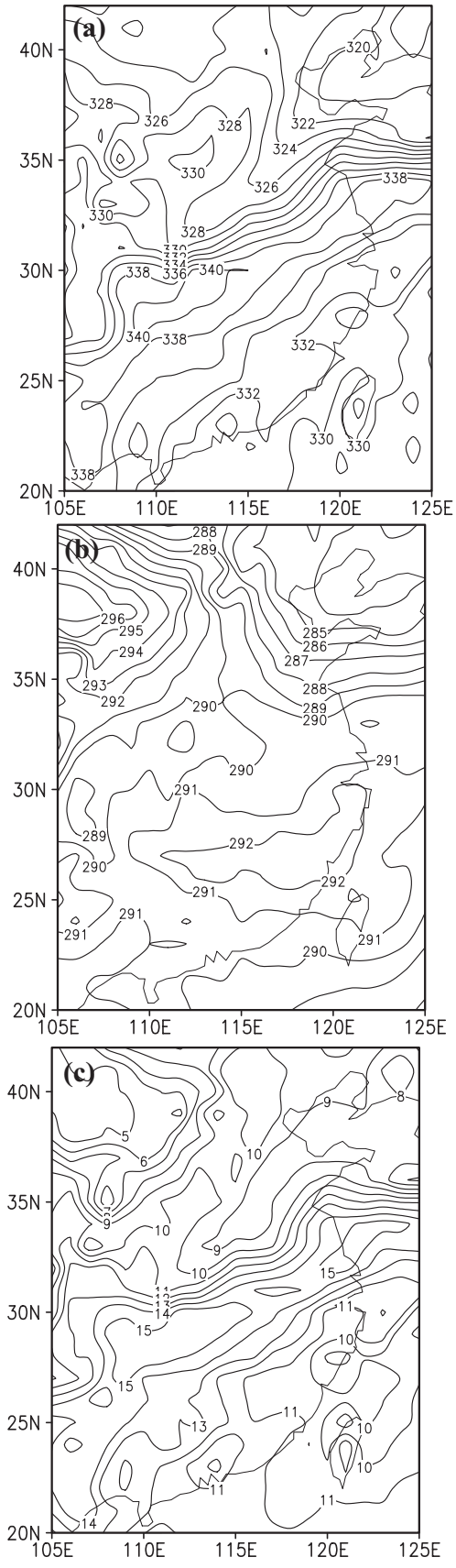

Fig. 3. (a) Equivalent potential temperature (K), (b) temperature (K), and (c) specific humidity (g kg^{-1}) at the 800 hPa level at 0000 UTC 10 July 2010.

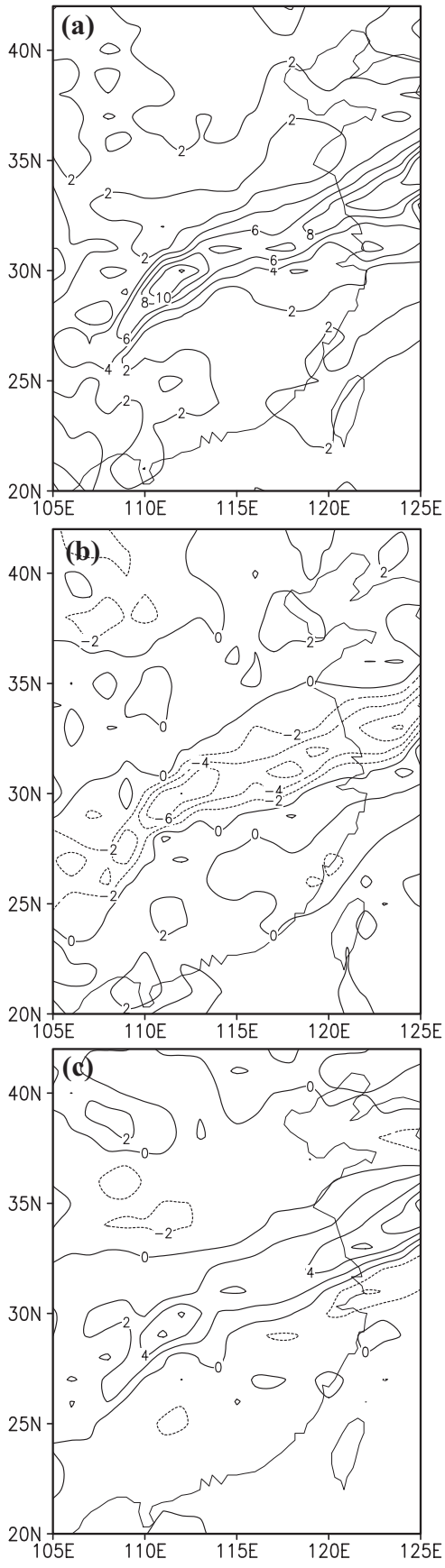

Fig. 4. (a) Resultant deformation, (b) divergence, and (c) vorticity (10^{-5} s^{-1}) at the 800 hPa level at 0000 UTC July 2010.

in Fig. 6b) and the deformation frontogenesis function (red line in Fig. 5c), and the maximal precipitation center (red rectangular box in Fig. 6c) and the intensity center of the deformation frontogenesis function (red rectangular box in Fig. 5e) located at (30°N, 110°E), do not appear in the distribution charts of the traditional frontogenesis function (Figs. 5d and f), even when the contour interval of both the deformation frontogenesis function (by reducing to 0.5) and the traditional frontogenesis function (by reducing to 0.1) are changed. This shows that the coverage of both frontogenesis functions is spread out and wider than those of the rainbands. However, the traditional function does not perform better. Note that no deformation frontogenesis signals in Fig. 5a cover the dashed-line part of the southern branch of double rainbands (east of 117°E and south of 29°N), which may be explained as follows. The calculation of the deformation frontogenesis function is based on the deformation field. The dashed-line part in Fig. 6a is outside the deformation-dominant confluence shear region (Figs. 2a and c), and therefore is not located in the large-value band of the deformation field (Fig. 4a). Thus, the deformation frontogenesis function based on the deformation field does not work at this location. It is possible that this represents one of the limitations of this kind of frontogenesis function, exerting its great advantage in the deformation-dominant flow pattern. Furthermore, the deformation frontogenesis strengthens [(3.5–6) $\times 10^{-14}$ m^{-1} s^{-2}] with the increase of rainfall amount (80–130 mm) from 10 to 11 July (Figs. 5a and e), while the traditional frontogenesis function [(3–1.5) $\times 10^{-9}$ K s^{-1} m^{-1}] (Figs. 5b and f) cannot reflect the variation in the rainfall amount (Figs. 6a and c).

Note that the area of the deformation frontogenesis function is a little larger than the rainband, which can be further explained by the following four aspects:

(1) The area of the deformation frontogenesis function is larger than the rainband, which is partly related to the choice of contour interval. If the contour interval of precipitation (Fig. 6) is changed (e.g., reduced to 1 mm), the rainbands become wider.

(2) The deformation frontogenesis function is based on the resultant deformation field, which after all is a pure dynamical variable. Precipitation events are very complicated processes related to clouds and microphysics, possibly partly explaining why their coverage does not completely match.

(3) Furthermore, the more important and useful aspect for precipitation is the prediction ability rather than the diagnosis. Therefore, the frontogenesis functions (Figs. 5a, c and e) are compared with the precipitation 6 h later (Fig. 6) to test their prediction ability. For example, the frontogenesis functions at 0000 UTC 10 July (Figs. 5a and b) are compared with precipitation at 0600 UTC 10 July (Fig. 6a), and the frontogenesis functions at 0600 UTC (Figs. 5c and d) are compared with 6 h precipitation at 1200 UTC (Fig. 6b), and so on. This may also partly explain why their coverage does not completely match.

(4) The correlation between the deformation frontogenesis function with precipitation should be compared with that of the traditional frontogenesis function with precipitation be-

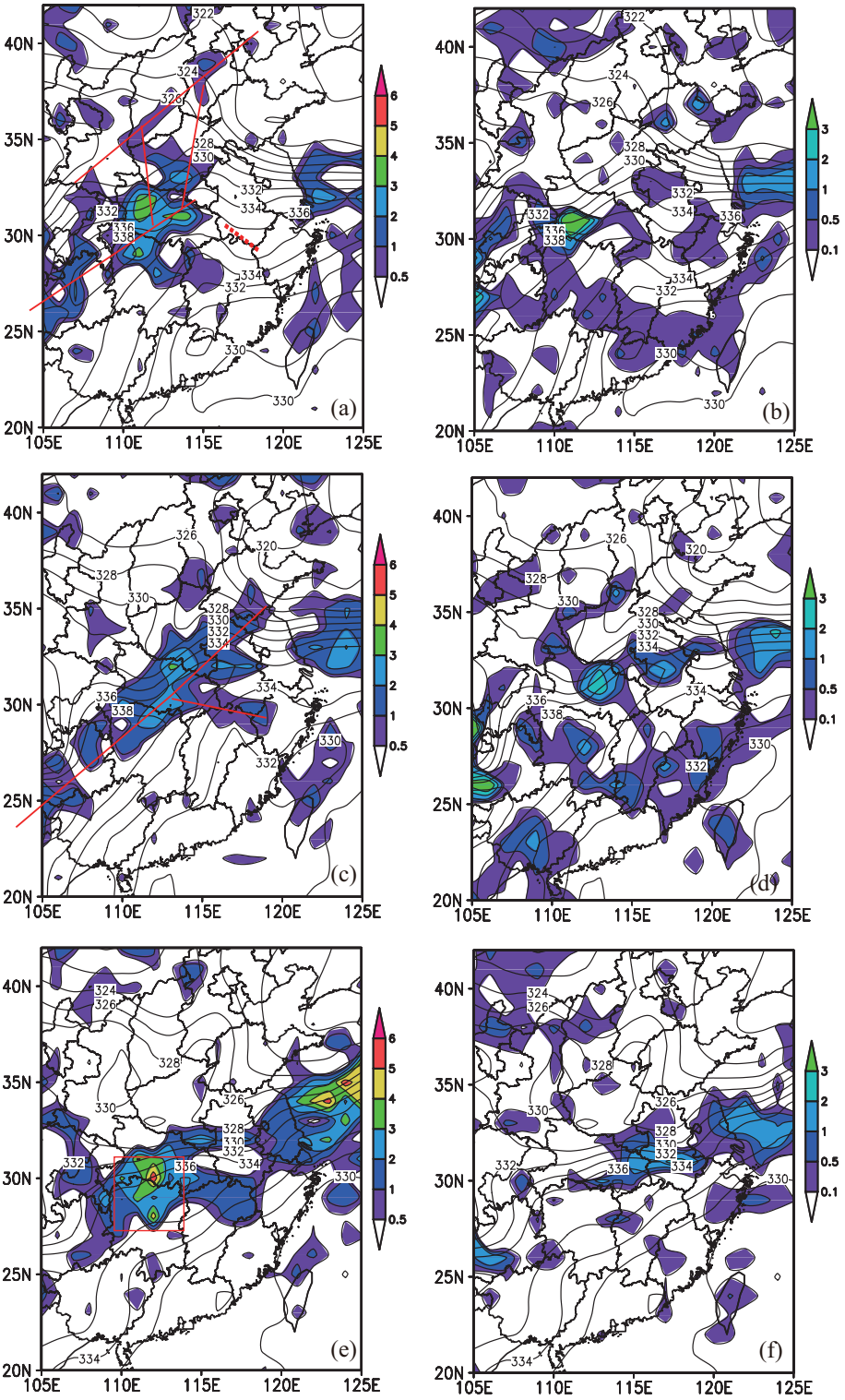

Fig. 5. Distributions of deformation frontogenesis (left column, 10^{-14} m^{-1} s^{-2}), traditional frontogenesis function (right column, 10^{-9} K s^{-1} m^{-1}) (shading represents frontogenesis), and equivalent potential temperature (isolines, K) at 800 hPa: (a, b) 0000 UTC 10; (c, d) 0600 UTC 10; (e, f) 0000 UTC 11 July 2010.

cause these two frontogenesis functions are equivalent—both have a role in frontogenesis and induce the development of weather systems and precipitation. By comparison, the deformation function without considering friction (which is difficult to accurately calculate) performs better than the traditional frontogenesis function when neglecting diabatic heating because it is too difficult to accurately calculate.

But why can the new deformation frontogenesis function

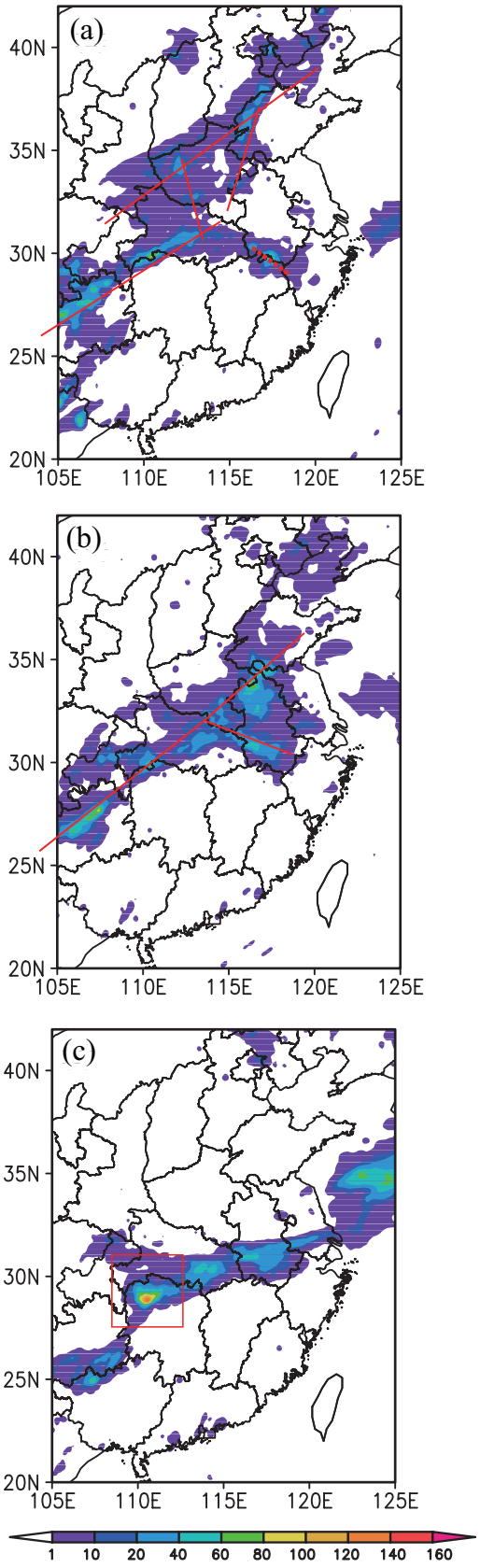

Fig. 6. Observed 6 h rainfall amount (mm) over the middle and lower reaches of the Yangtze River at (a) 0600 UTC 10, (b) 1200 UTC 10, and (c) 0600 UTC 11 July 2010.

reflect the frontogenesis process better than the traditional function? Because from the above analyses the resultant deformation can drive the contraction of θ_e isolines, the problem of frontogenesis is considered from the dynamic rather than the thermodynamic aspect in this paper. From the connections and interactions among E, θ_e (Fig. 7a) and ω (Fig. 7b), the mechanism is further explained as follows. According to traditional understanding, the confluence associated with the deformation and the transportation of warm and moist air by such a flow makes the mass and moisture concentrated distinctly towards the confluence region of the saddle field. Therefore, the θ_e isolines become dense, indicating a buildup of strong θ_e gradient along the confluence zone, i.e. frontogenesis (Fig. 7a). In the 3D case, vertical motion along the confluence zone will cause the upward transportation of warm and moist air brought in by the horizontal deformation flow. Furthermore, the difference in vertical motion inside and outside the frontal zone (Fig. 7b) induced by the deformation flow makes a difference in the pumping up of low-level air, which will cause low-level convergence and thus increase the horizontal gradient of θ_e. Thus, frontogenesis presents and it sets up a favorable condition for precipitation, which possibly offers an explanation. Furthermore, the deformation frontogenesis function avoids the influence of inaccuracy brought about by the calculation of the diabatic heating term in the traditional frontogenesis formulation.

Figure 8 shows the variations of the terms in the deformation frontogenesis function [in Eq. (20)]. The evolution tendency of the terms (Fig. 8) shows that, although the Coriolis forcing term (X_3) is negative and nearly equal to zero, the advection forcing term (X_1) and the pressure gradient forcing term (X_2) in the frontal zone work together to sustain the strong gradient of θ_e, which manifests the major factors affecting deformation frontogenesis. The results of this case show that the focus of the mass field towards the confluence zone, caused by the advection forcing effect of deformation frontogenesis, has some positive feedback on the pressure gradient between both sides of the confluence zone. Therefore, the pressure gradient forcing is related to the change of local deformation frontogenesis. Certainly, to begin with, it is the confluence associated with the advection forcing that provides a favorable condition for moisture convection. The fact that the advection forcing term is the largest in magnitude in this case further emphasizes the role of the wind field, which also verifies the appropriateness of directly defining a frontogenesis function from the dynamical viewpoint, since it is the wind field that drives the compactness of the isolines of any one tracer to lead to frontogenesis.

6. Conclusion

In this study, we investigated a mei-yu front using a new deformation frontogenesis function. The new frontogenesis function is defined based on the local change rate of the absolute gradient in the resultant deformation. Different from the traditional frontogenesis function, the new deformation

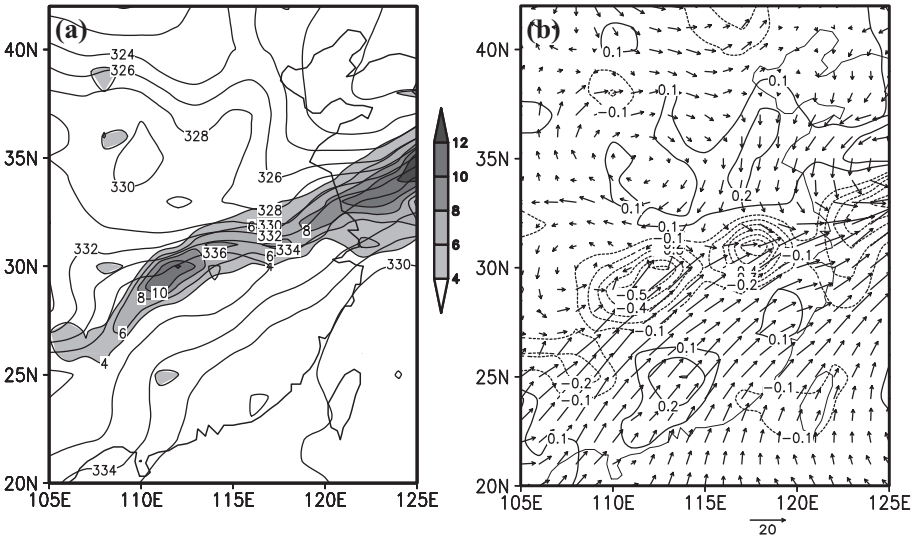

Fig. 7. (a) Distributions of resultant deformation (10^{-5} s^{-1}, shaded regions indicate values of more than 4.0) and equivalent potential temperature (isolines, K) at the 800 hPa level; (b) vertical speed (hPa s^{-1}, isolines, negative values denote upward motion) and horizontal wind vectors (m s^{-1}) at 0000 UTC 11 July 2010.

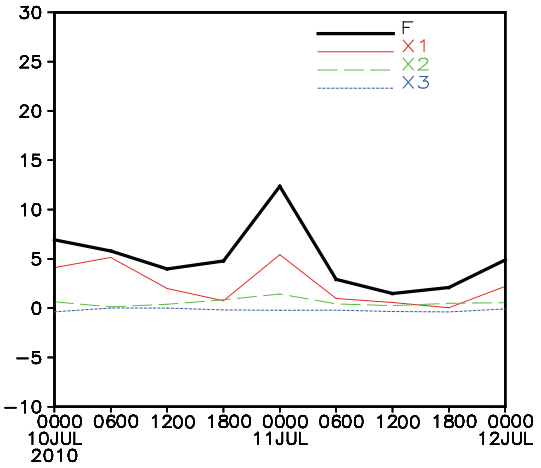

Fig. 8. Variation of the area-averaged (28°–31°N, 110°–120°E) terms in the deformation frontogenesis function [refers to Eq. (20), X_1: advection forcing term; X_2: pressure gradient forcing term; X_3: Coriolis forcing term (units: 10^{-15} m^{-1} s^{-2})] at 800 hPa from 0000 UTC 10 to 0000 UTC 12 July 2010. ($F = X_1 + X_2 + X_3$).

frontogenesis function places emphasis on the flow itself rather than on the flow-driving tracers, such as potential temperature or equivalent potential temperature. Such a definition of the frontogenesis function is independent of the tracer type, and thus can be used in situations where a temperature/moisture front occurs in the absence of a moisture/temperature front. Therefore, it is more intuitive for the study of mei-yu frontogenesis since the isolines of both temperature and moisture are derived by deformation in a deformation-dominant flow pattern.

Within the framework of quasigeostrophic theory, an ω-equation was derived, with shearing and stretching deformation presented as forcing functions. This result suggested an importance of deformation in frontal circulation.

A deformation-frontogenesis function was derived and applied to a mei-yu front precipitation case. In comparison with traditional frontogenesis dynamics, which evaluate the local change rate of the absolute gradient of equivalent potential temperature, the deformation-frontogenesis equation presented a better depiction of fronts in deformation-dominant flow situations. More importantly, the deformation frontogenesis regions covered the rainband well and showed close correlation with the precipitation pattern, which is significant in terms of the prognosis of precipitation.

To obtain more general conclusions and to explore the relationship between deformation frontogenesis and precipitation in more detail, we plan in future work to examine more cases using data with higher temporal and spatial resolutions.

Acknowledgements. The authors were supported by the National 973 Fundamental Research Program of the Ministry of Science and Technology of China (Grant No. 2013CB430105), the Key Research Program of the Chinese Academy of Sciences (Grant No. KZZD-EW-05-01), the Special Scientific Research Fund of the Meteorological Public Welfare of the Ministry of Sciences and Technology, China (Grant No. GYHY201406003), the National Natural Science Foundation of China (Grant Nos. 41375054, 41375052 and 40805001), and the Opening Foundation of the State Key Laboratory of Severe Weather, Chinese Academy of Meteorological Sciences (Grant Nos. 2012LASW-B02 and 2013LASW-A06).

REFERENCES

Bergeron, T., 1928: Uber die dreidimensional Verkniipfende Vetteranalyse. *I. Geof. Publ.*, **5**(6), 1–111. (in Germany)

Bluestein, H. B., 1992: *Synoptic-dynamic Meteorology in Midlati-*

tudes. Vol. I, *Principles of Kinematics and Dynamics*, Oxford University Press, USA, 430 pp.

Davies-Jones, R. P., 1982: Observational and theoretical aspects of tornadogenesis. *Intense Atmospheric Vortices*, L. Bengtsson and J. Lighthill, Eds., Springer-Verlag, 175–189.

Davies-Jones, R. P., 1985: Comments on "A kinematic analysis of frontogenesis associated with a nondivergent vortex." *J. Atmos. Sci*., **42**, 2073–2075.

Doswell, C. A., III, 1984: A kinematic analysis of frontogenesis associated with a nondivergent vortex. *J. Atmos. Sci*., **41**, 1242–1248.

Eliassen, A., 1962: On the vertical circulation in frontal zones. *Geofys. Publ*., **24**(4), 147–160.

Fang, J., and R. S. Wu, 1998: Frontogenesis, evolution and the time scale of front formation. *Adv. Atmos. Sci.*, **15**, 233–246 doi.

Fang, J., and R. S. Wu, 2001: Topographic effect on geostrophic adjustment and frontogenesis. *Adv. Atmos. Sci.*, **18**, 524–538 doi.

Gao, S. T., S. Yang, M. Xue, and C. G. Cui, 2008: The total deformation and its role in heavy precipitation events associated with deformation-dominant flow patterns. *Adv. Atmos. Sci.*, **25**, 11–23, doi: 10.1007/s00376-008-0011-y.

Gao, S. T., S. Yang, and B. Chen, 2010: Diagnostic analyses of dry intrusion and nonuniformaly saturated instability during a rainfall event. *J. Geophys. Res.*, **115**, D02102, doi: 10.1029/2009JD012467.

Hoskins, B. J., and F. P., Bretherton, 1972: Atmospheric frontogenesis models: Mathematical formulation and solution. *J. Atmos. Sci*., **29**, 11–37.

Keyser, D., M. J. Pecnick, and M. A. Shapiro, 1986: Diagnosis of the role of vertical deformation in a two-dimensional primitive equation model of upper-level frontogenesis. *J. Atmos. Sci*., **43**, 839–850.

Keyser, D., J. M., Reeder, and J. R., Reed, 1988: A generalization of Petterssen's frontogenesis function and its relation to the forcing of vertical motion. *Mon. Wea. Rev.*, **116**, 762–780.

Li, N., L. K. Ran, Y. S. Zhou, and S. T. Gao, 2013: Diagnosis of the frontogenesis and slantwise vorticity development caused by the deformation in the Beijing "7.21" torrential rainfall event. *Acta Meteorologica Sinica*, **71**, 593–605.

Margules, M., 1906: Uber temperaturschichtung in stationar bewegter und ruhender luft Hann-Band. *Meteorol. Z.*, 243–254. (in Germany)

Miller, J. E., 1948: On the concept of frontogenesis. *J. Meteor.*, **5**, 169–171.

Newton, C. W., 1954: Frontogenesis and frontolysis as a three-dimensional process. *J. Atmos. Sci.*, **11**, 449–461.

Ninomiya, K., 1984: Characteristics of Baiu front as a predominant subtropical front in the summer northern hemisphere. *J. Meteor. Soc. Japan*, **62**, 880–893.

Ninomiya, K., 2000: Large-and meso-scale characteristics of Meiyu/Baiu front associated with intense rainfalls in 1–10 July 1991. *J. Meteor. Soc. Japan*, **78**, 141–157.

Norbury, J., 2002. *Large-scale Atmosphere-Ocean Dynamics*. Vol I, Cambridge University Press, 2–7.

Petterssen, S., 1936: Contribution to the theory of frontogenesis. *Geofys. Publ.*, **11**(6), 1–27.

Petterssen, S., 1956: *Weather Analysis and Forecasting.* Vol.1, *Motion and Motion Systems*, 2nd ed., McGraw-Hill, 428 pp.

Ran, L. K., W. X. Yang, and Y. C. Hong, 2009: Deformation of moisture flux circulation surrounding the landfall typhoon "Bilis". *J. Trop. Meteor.*, **15**, 167–180, doi: 10.3969/j.issn.1006-8775.2009.02.006.

Reed, R. J., 1955: A study of a characteristic type of upper-level frontogenesis. *J. Atmos. Sci*., **12**, 226–237.

Reed, R. J., and E. F. Danielsen, 1958: Fronts in the vicinity of the tropopause. *Arch. Much. Meteor. Geophys. Bioklim.*, **11**, 1–17.

Sawyer, J. S., 1956: The vertical circulation at meteorological fronts and its relation to frontogenesis. *Proc. Roy. Soc. London A.*, **234**, 346–362.

Schultz, D. M., and W. J. Steenburgh, 1999: The formation of a forward-tilting cold front with multiple cloud bands during superstorm 1993. *Mon. Wea. Rev.*, **127**, 1108–1124.

Schultz, D. M., and F. Sanders, 2002: Upper-level frontogenesis associated with the birth of mobile troughs in northwesterly flow. *Mon. Wea. Rev.*, **130**, 2593–2610.

Schultz, D. M., and R. J. Trapp, 2003: Nonclassical cold-frontal structure caused by dry subcloud air in northern Utah during the intermountain precipitation experiment. *Mon. Wea. Rev.*, **131**, 2222–2246.

Schultz, D. M. D. Keyser, and L. F. Bosart, 1998: The effect of large-scale flow on low-level frontal structure and evolution in midlatitude cyclones. *Mon. Wea. Rev.*, **126**, 1767–1791.

Wu, R. S., and J. Fang, 2001: Mechanism of balanced flow and frontogenesis. *Adv. Atmos. Sci*., **18**, 323–334.

Wu, R. S., S. T. Gao, and Z. M. Tan, 2004: *Front and Meso-scale Disturbation.* China Meteorological Press, Beijing, 6–57.

Yang, S., 2007: The study of the formation mechanism of heavy rain events occurred in Huabei areas in China. Ph.D. dissertation, Graduate University of Chinese Academy of Sciences, Beijing, 109 pp.

Yang, S., S. T. Gao, and D. H. Wang, 2007: Diagnostic analyses of the ageostrophic Q vector in the non-uniformly saturated, frictionless, and moist adiabatic flow. *J. Geophys. Res.*, **112**, D09114, doi: 10.1029/2006JD008142.

Yang, S., X. P. Cui, L. K. Ran, 2009: Analyses of dry intrusion and instability during heavy rainfall event occurred in Northern China. *Atmos. Oceanic Sci. Lett.*, **2**, 108–112.

Yang, S., S. T. Gao, and C. G. Lu, 2014: A generalized frontogenesis function and its application. *Adv. Atmos. Sci.*, **31**, 1065–1078, doi: 10.1007/s00376-014-3328-y.

Yu, F., S. M. Fu, S. X. Zhao, and J. H. Sun, 2012: Study on the dynamic characteristics of an eastward-offshore mesoscale vortex along the Meiyu-Baiu Front. *Atmos. Oceanic Sci. Lett.*, **5**, 360–366.